Electronic structures, bonding natures and defect processes in Sn-based 211 MAX phases

Hadi, M. A., Kelaidis, N., Naqib, S. H., Chroneos, A. & Islam, A. K. M. A.

Original citation & hyperlink:
Hadi, MA, Kelaidis, N, Naqib, SH, Chroneos, A & Islam, AKMA 2019, 'Electronic structures, bonding natures and defect processes in Sn-based 211 MAX phases', Computational Materials Science, vol. 168, pp. 203-212.
https://dx.doi.org/10.1016/j.commatsci.2019.06.008

DOI 10.1016/j.commatsci.2019.06.008
ISSN 0927-0256

Publisher: Elsevier

Electronic structures, bonding natures and defect processes in Sn-based 211 MAX phases

M.A. Hadi, [1*] N. Kelaidis,[2,3] S. H. Naqib,[1] A. Chroneos,[2,4†] A. K. M. A. Islam[1,5]

[1]Department of Physics, University of Rajshahi, Rajshahi 6205, Bangladesh
[2]Faculty of Engineering, Environment and Computing, Coventry University, Priory Street, Coventry CV1 5FB, UK
[3]Theoretical and Physical Chemistry Institute, National Hellenic Research Foundation,Vass. Constantinou 48, GR-11635 Athens, Greece
[4]Department of Materials, Imperial College, London SW7 2AZ, UK
[5]International Islamic University Chittagong, Kumira, Chittagong-4318, Bangladesh

Abstract

The electronic structure, bonding natures, and defect processes of the new superconducting MAX phase Lu_2SnC are investigated by using density functional theory, and are compared to other existing M_2SnC phases. The formation of M_2SnC MAX phases is exothermic and these compounds are intrinsically stable in agreement with experiment. The finite value of DOS, in addition to the d-resonance at the vicinity of the Fermi level, indicates a metallic nature and conductivity of M_2SnC MAX phases. The strength of the covalent M–C bond is higher than that of the covalent M–Sn bond. The calculated effective valence charge also indicates the dominance of covalency in the chemical bonding in the studied compounds. The charge transfer in M_2SnC phases indicates the ionic nature of their chemical bonds. The ionic character of their chemical bonds can also be understood from the spherical nature of charge distribution in their contour maps of electron charge density. Therefore, the overall bonding nature in the studied M_2SnC MAX phases is a combination of metallic, covalent, and, ionic. The bond length is directly proportional to the crystal radius, while bond covalency is inversely proportional to the crystal radius. Additionally, the Fermi surface topology is also investigated. Considering the intrinsic defect processes it is calculated that Nb_2SnC is the material that is predicted to have better radiation tolerance.

Key-words: Sn-based 211 MAX phase; Electronic structure; Bonding nature; Defect process

1. Introduction

MAX phases, a new class of ternary layered carbide and nitride materials, are potentially technologically important as they exhibit unique physical properties due to the combination of metallic and ceramic natures [1]. In the mid-sixties of the last century, Nowotny *et al.* first discovered some members of this family, now known as the '211' MAX phases, and named them 'H' phases [2]. After re-synthesizing a phase pure dense Ti_3SiC_2 and its characterizing study in 1996 by Barsoum and El-Raghy, a renewed interest of scientific community has grown on MAX phases [3]. Following this study, Barsoum *et al.* also discovered the carbide phase Ti_4AlN_3 and understood that they were dealing with a larger family of compounds with similar properties [4–6]. This realization led to the nomenclature "$M_{n+1}AX_n$" (later shortened to MAX) phases, which also stands for the chemical formula for this class of solids [1,7]. In this formula, M represents a transition metal, A refers to an A-group element, and X is carbon and/or nitrogen. The MAX phases are categorized into different sub-families, namely 211, 312, and 413 phases depending on n = 1, 2, and 3, respectively.

MAX phases possesses a diverse combination of some of the best physical, chemical, electrical, and mechanical properties, showing both metallic and ceramic physiognomies. In the meantime, a tremendous progress has been made in understanding the properties of these layered compounds [1,3–23]. The MAX phases have been characterized having properties found commonly in metals such as high thermal and electrical conductivities, thermal shock resistance, damage tolerance, machinability and plasticity at high temperature [1,14–17]. Remarkably, ceramic-like properties are also present by such as light weight, elastic rigidity, fatigue, oxidation and corrosion resistant, and maintaining the strength to high temperature [18–23]. Due to these technologically important properties, MAX phases are potentially used as tough, machinable and thermal shock refractories, high temperature heating elements, coatings for electrical contacts, neutron irradiation resistant parts for nuclear applications, precursors for synthesis of carbide-derived carbon and MXenes, the latter being a family of two-dimensional transition metal carbides, nitrides, and carbonitrides [24–28].

* Corresponding author: M.A. Hadi (hadipab@gmail.com)
† Corresponding author: A. Chroneos (ab8104@coventry.ac.uk)

MAX phases crystallize in the layered hexagonal structures with space group $P6_3/mmc$ (no. 194). These materials comprise of alternate near-close-packed layers of M_6X octahedra interpolated with pure A-atomic layers. The M_6X octahedra, similarly to those materializing in the corresponding MX binary phases, are linked to each other by edge sharing [29]. The number of M-layers separating every two A-layers leads to the basic difference in the structures of 211, 312, and 413 MAX phases. In fact, in the 211, 312, and 413 phases, two, three, and four M-layers exist in the middle of every two A-layers. Such atomic arrangements in the MAX phases give them a characteristic layered structure, which accumulates both metallic and ceramic properties in these solids. For this reason, the MAX phases are sometimes termed as 'metallic ceramics'. These compounds are also termed as 'nanolaminates' due to their effective laminated monolayers [30].

A large number of MAX phases have been predicted very recently [12]. The list of existing MAX phases is expanding day by day by synthesizing the new members [31–34]. Recently, a new MAX phase Lu_2SnC, out of any prediction, is synthesized by Kuchida *et al*. [35]. It is not only new but also exceptional as it contains Lu belonging to lanthanide series instead of transition metals. Kuchida *et al*. [35] applied the arc melting method to prepare a polycrystalline sample of Lu_2SnC. Powder X-ray diffraction (PXRD) pattern is employed to index the unit cell. The cell is identified as a hexagonal system with Cr_2AlC-type structure and with the space group of $P6_3/mmc$, which belongs to the MAX phase. They also reported the occurrence of superconductivity at 5.2 K for Lu_2SnC on the basis of their magnetic susceptibility and electrical resistivity measurements. The new phase Lu_2SnC should belong to the type-II superconductors according to the obtained superconducting parameters.

In our previous paper [36], the structural, elastic, mechanical and thermal properties of Lu_2SnC are investigated along with other existing M_2SnC (M = Ti, Zr, Hf, Nb) phases and the obtained results are compared with those found in literatures. It is mentioned that the early existing phase Nb_2SnC is also superconductor and its superconducting transition temperature is 7.8 K. The electronic structure and bonding nature of Lu_2SnC are still unexplored. The defect processes in existing M_2SnC phases have yet to be studied. The knowledge of electronic structure is important to understand many physical properties of crystals. The investigation of defect processes is important to provide a primary selection criterion for radiation tolerance on the basis of Schottky or Frenkel pair formation energies. Motivated by this we have done the present study.

2. Computational methods

The CASTEP code [37] embodied with planewave pseudopotential density functional theory (DFT) [38,39] is employed to carry out the present investigation. Generalized gradient approximation (GGA) simplified by Perdew-Burkey-Ernzerhof (PBE) is used to treat the electronic exchange and correlation potential [40]. The interactions of electrons with ion cores are evaluated with the Vanderbilt type ultrasoft pseudopotential [41] with $2s^2 2p^2$, $5s^2 5p^2$, $5d^2\ 6s^2$, $5p^6\ 5d^1\ 6s^2$, $4p^6\ 4d^4\ 5s^1$, $3p^6\ 3d^2\ 4s^2$, and $4p^6\ 4d^2\ 5s^2$ as the basis set of the valence electron states for C, Sn, Hf, Lu, Nb, Ti, and Zr, respectively. A Γ-centered k-point mesh of 15×15×3 grid in Monkhorst-Pack (MP) scheme [42] is applied in the reciprocal space for sampling the first Brillouin zone of hexagonal unit cell for MAX phase. A planewave basis with a cutoff energy of 700 eV is used to expand the eigenfunctions of the valence and nearly valence electrons. To minimalize the total energy and internal forces the Broyden-Fletcher-Goldfarb-Shanno (BFGS) algorithm is used in the geometry optimization [43]. The convergence tolerance for total energy, residual force, maximum ionic displacement, and maximum stress are set to 5×10^{-6} eV/atom, 0.01 eV/Å, 5×10^{-4} Å, and 0.02 GPa, respectively. For self-consistent field calculations, the tolerance is chosen 5×10^{-7} eV/atom. To obtain smooth Fermi surfaces a k-point mesh of 15×15×3 grid in MP scheme is used. DFT is an appropriate method to describe the electronic structure of crystalline solids [30,36,44–65].

To carry out the population analysis using the CASTEP code, a projection of the planewave states onto a localized (LCAO) basis is used through a scheme proposed by Sanchez-Portal *et al*. [66]. Population analysis of the resulting projected states is then implemented with the Mulliken formalism [67]. The defect calculations are carried out with a 108-atomic site supercell using a 3 × 3 × 1MP k-point mesh under constant pressure. Considering all possible interstitial sites, we performed an intensive computational search to identify the potential interstitial sites. The defect energies are defined as effectively energy differences (refer to defect reactions in section 3.4) between isolated defects. The effectiveness of the technique to determine the defect properties and the convergence as compared to experiment has been discussed in a recent study [68].

3. Results and discussion

3.1. Optimized Geometry and energy

The optimized geometry of newly synthesized Lu_2SnC as a structural model of M_2SnC 211 MAX phases is shown in Fig. 1. The calculated lattice constants *a* and *c* along with experimental [35, 69,70] and other theoretical [71–73] values are plotted in Fig. 2. It is observed that the present values are very close to the experimental ones. The deviation of present values from the experimental values for *a* and *c* of Lu_2SnC is 0.91% and 1.08%, respectively. For other M_2SnC phases, the deviation of *a* and *c* is calculated to be within 0.27–1.66% and 0.71–1.12%, respectively. These ensure the reliability of the present calculations. The GGA-trend, overestimation in lattice constants, is also observed in the present CASTEP-GGA and previous VASP-GGA [71] calculations. All results for lattice constants of M_2SnC phases including Lu_2SnC show increasing trend following the sequence of M-elements as Ti→Nb→Hf→Zr→Lu, excepting the results due to Bouhemadou [73]. Both the lattice parameters *a* and *c* and consequently the unit cell volume *V* are largest for Lu_2SnC among all existing M_2SnC phases. In our previous paper, we showed that the crystal radius of M-element plays the role for this trend [36].

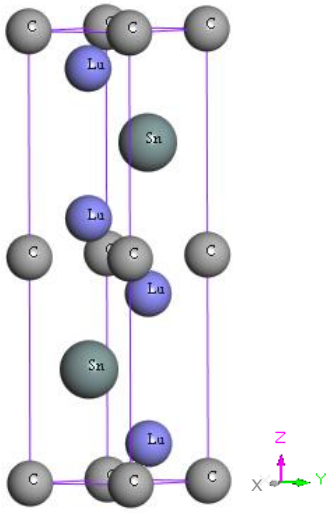

Fig. 1. Geometry of Lu_2SnC as a structural model of M_2SnC.

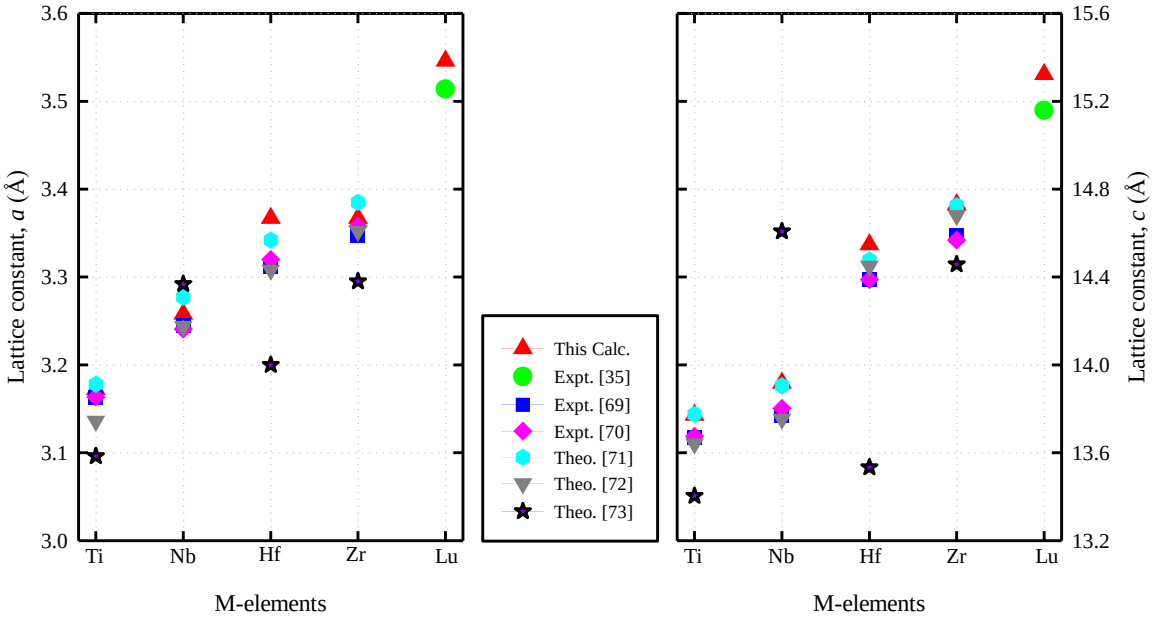

Fig. 2. Lattice constants *a* and *c* of M_2SnC as a function of M-elements.

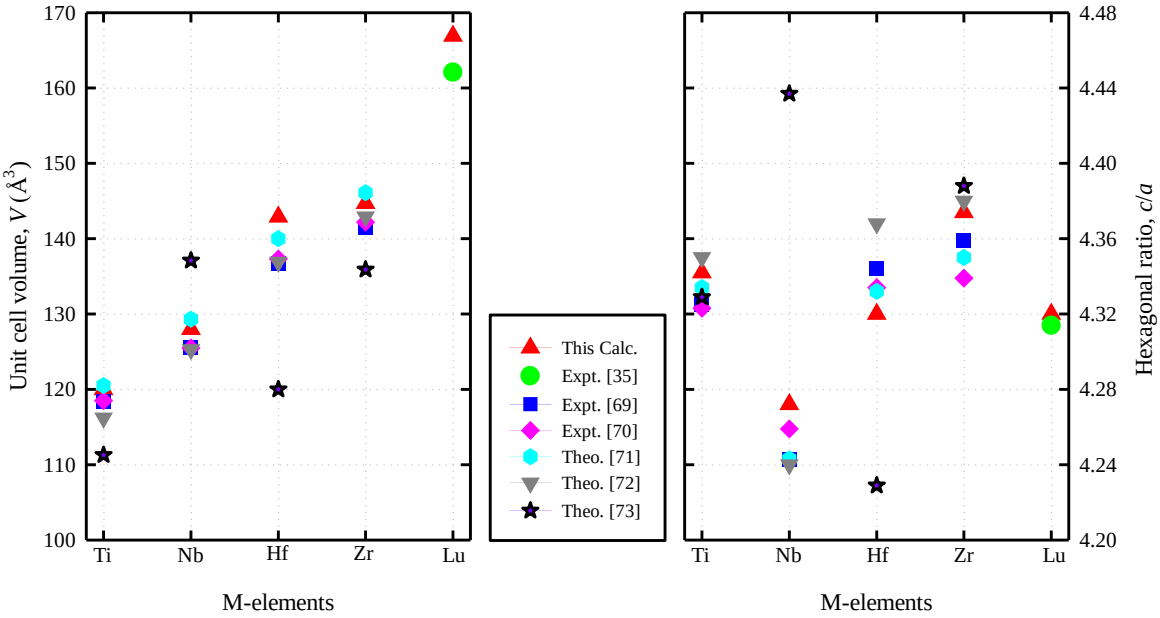

Fig. 3. Unit cell volume and hexagonal ratio of M_2SnC as a function of M-elements.

The calculated unit cell volume and hexagonal ratio are shown in Fig. 3 together with other literature values. The cell volume also exhibits the similar trend as observed in lattice constants. This trend actually follows the increasing trend of crystal radius of M-elements [36]. Though the hexagonal ratio *c*/*a* lies within the range 3.5–4.6 for 211 MAX phases, the literature values found in Ref. [73] scatter randomly. As the present lattice constants are consistent with the experimental values, the present volume and hexagonal ratio also show the closeness to the measured ones. The internal energy, $E(V)$ for M_2SnC crystal systems are calculated with the equation of state [74] and shown in Fig. 4.

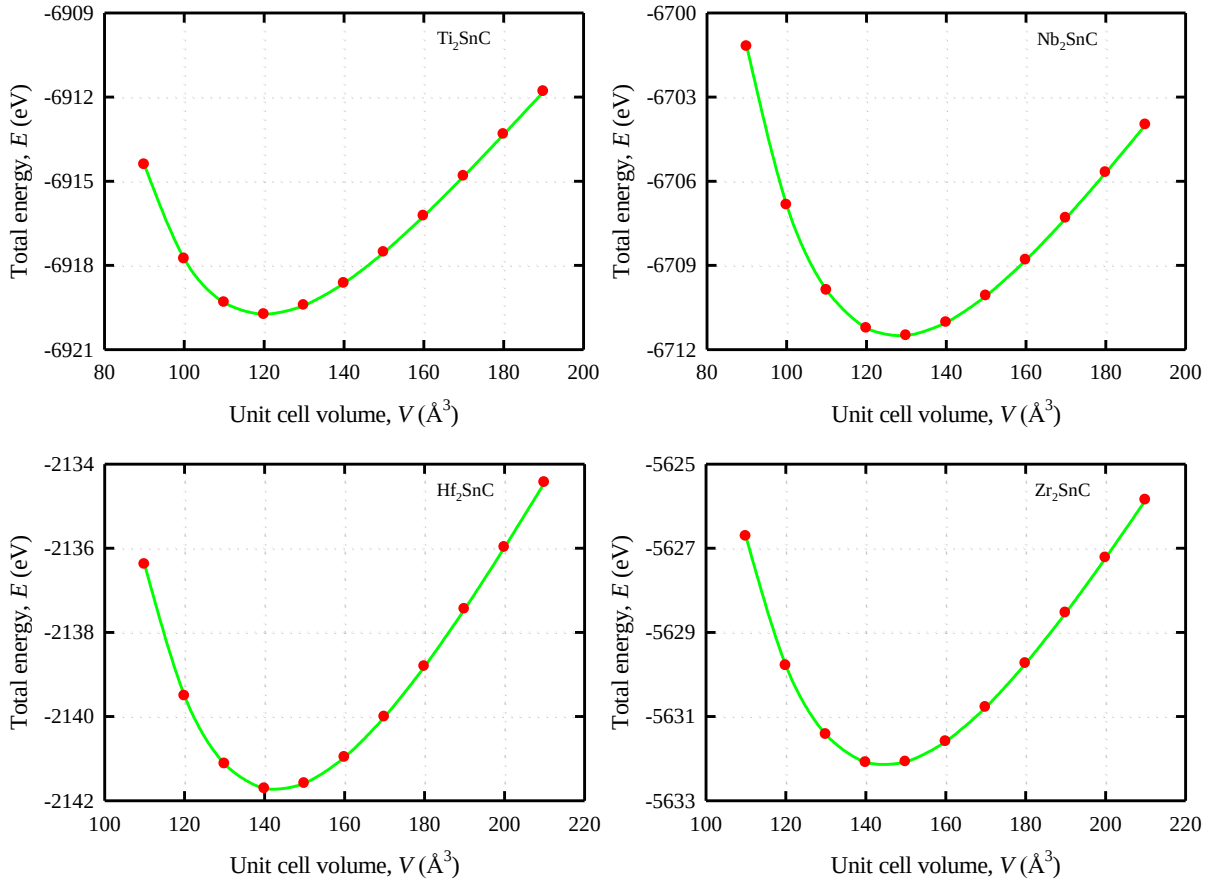

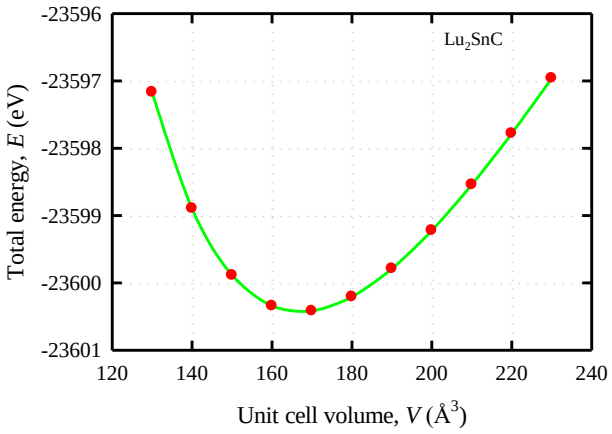

Fig. 4. Energy-volume relationship for M_2SnC MAX phases.

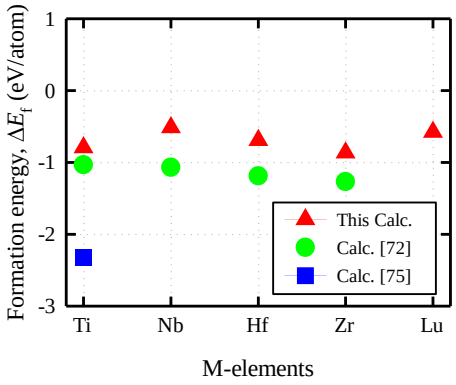

Fig. 5. Formation energies for M_2SnC MAX phases.

The formation energy ΔE_f is calculated from the total energy of an examined phase minus the sum of the energies of its pure constituent elements. The calculated formation energies of Ti_2SnC, Nb_2SnC, Hf_2SnC, Zr_2SnC and Lu_2SnC are found to be -3.18, -2.05, -2.77, -3.47 and -2.31 eV/fu, respectively. These values are compared in Fig. 5 with those found in literatures [72,75]. Negative sign in these values imply that the materialization of M_2SnC MAX phases is exothermic and these compounds are intrinsically stable in covenant with the experiment [35,69,70]. Evidently, Zr_2SnC is the most stable phase. Between two superconducting phases, Lu_2SnC is more stable than Nb_2SnC.

3.2. Electronic band structure and density of states

Electronic band structures of five Sn-containing M_2SnC MAX phases are investigated with high symmetry points in the first Brillouin zone and shown in Fig. 6. The energy scale is defined with E-E_F and the Fermi surfaces are set at zero in this scale. No band gap arises in the energy band structures as a large number of valence bands cross over the Fermi level and overlap with the conduction bands. As a result, all the studied M_2SnC phases should attain metallic conductivity. Though the band profiles of M_3SnC_2 are almost similar [44], a distinct difference is observed for M_2SnC. The position of Fermi surface in Ti_2SnC is just below the valence band maximum near the Γ-point. In Nb_2SnC, it lies above the valence band maximum at the same point. The Γ-point, where the maximum valence bands meet together, situates above the Fermi level of Hf_2SnC, Zr_2SnC and Lu_2SnC MAX phases. The upward distances of these points from Fermi levels follow the order Zr_2SnC < Hf_2SnC < Lu_2SnC. A large number of valence bands accumulate around the energy levels of -4.3 eV in Lu_2SnC and leads to a large peak in the total DOS. Such accumulations are not found in the other M_2SnC phases although similar features in the band profiles are observed in Hf_2SnC and Zr_2SnC phases.

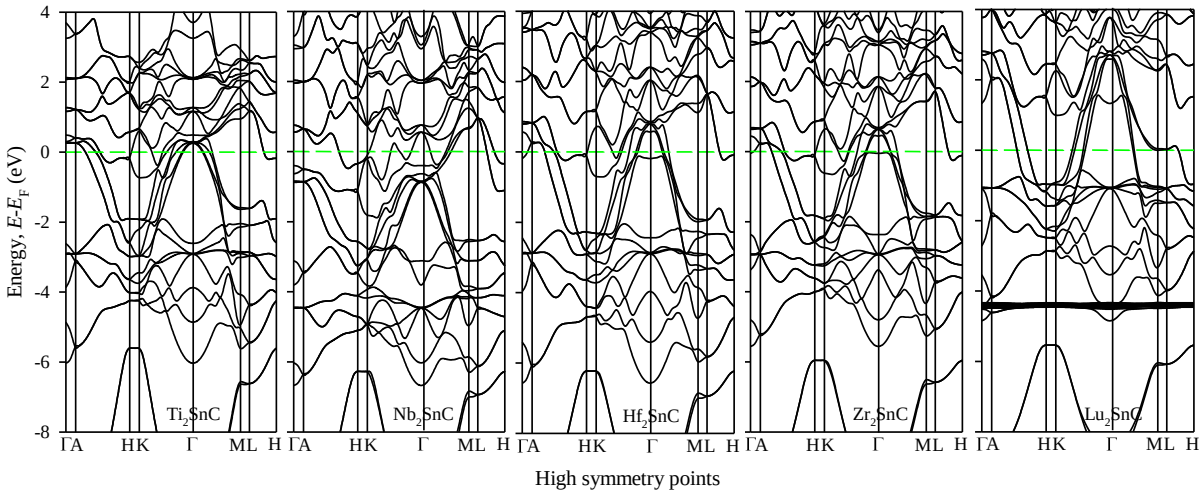

Fig. 6. Energy band structures for M_2SnC MAX phases.

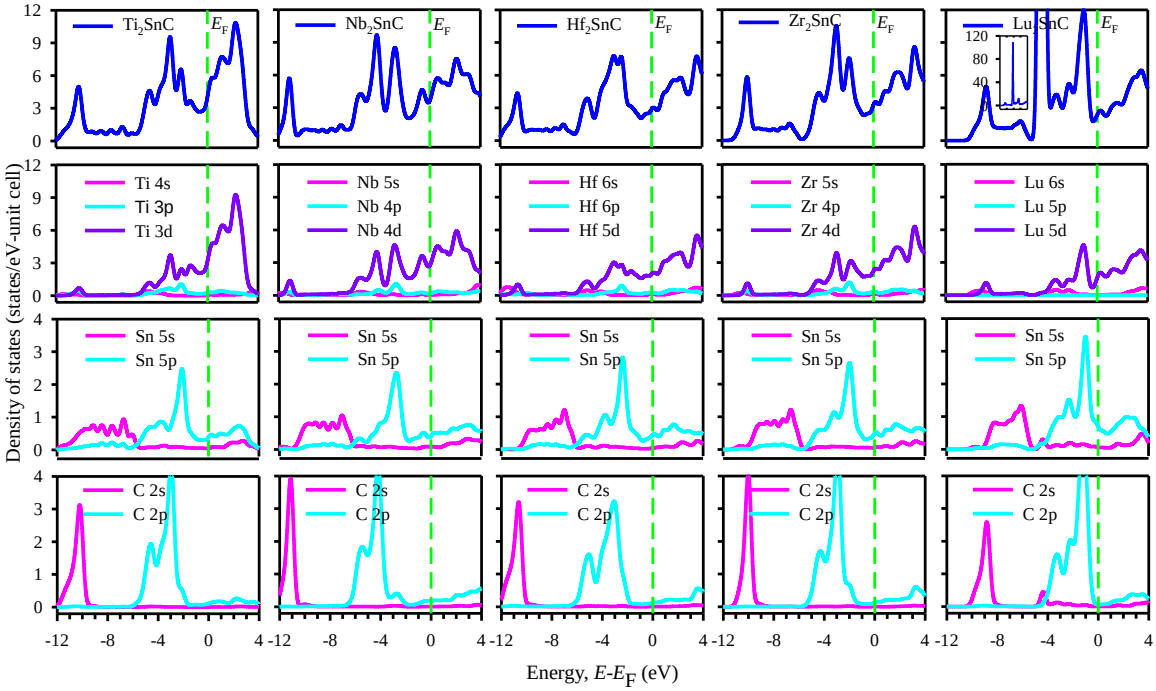

Fig. 7. Total and partial density of states of M_2SnC MAX phases.

The electronic density of states (DOS) provides more insights into the chemical bonding in crystals. The calculated total and partial DOS for M_2SnC including newly synthesized Lu_2SnC are shown in Fig. 7. The Fermi level E_F of Lu_2SnC lies near a pseudogap at the left similar to the other M_2SnC MAX phases, indicating their structural stability. The DOS has finite value at the Fermi level of each examined Sn-containing 211 MAX phases. Contribution to this finite value mainly comes from d-orbitals of each transition metal M. The finite value of DOS as well as d-resonance at the vicinity of the Fermi level is responsible for the metallic conductivity of these nanolaminates. The DOS at Fermi level is calculated to be 3.93, 3.62, 2.84, 3.25, and 2.35 states/eV-uc for Ti, Nb, Hf, Zr, and Lu based M_2SnC compounds. These values are compared with the literature values in Fig. 8. It is evident that the new phase Lu_2SnC has the lowest DOS at E_F, which is two-third of that of superconducting phase Nb_2SnC. Surprisingly, the T_c of Lu_2SnC (5.2 K) [35] is almost two-third of that of Nb_2SnC (7.8 K) [76]. To the best of our knowledge, presently there is no direct correlation between DOS at the Fermi surface and the superconducting transition temperature T_c. Whether it is a coincidence or an inherent relationship- more data should be examined for being sure. In a next paper we will examine for all superconducting MAX phases.

The valence band of M_2SnC phases studied here consists of main two parts. A low flat-type valence band arises between these two parts owing to s- electrons of the Sn-atoms similar to the M_3SnC_2 compounds [44]. The lower part with a single peak arises due to the hybridization between M d and C s electrons, indicating covalent M-C bonding in M_2SnC compounds. This part shifts towards the Fermi level as M-atom varies from Ti to Lu following the route Ti → Nb → Hf → Zr → Lu, which means that the covalency of M-C bonding i.e., M_2SnC phases, decreases following this order. Accordingly, Lu-based Lu_2SnC should be softer than other studied M_2SnC phases, which is consistent with the prediction based on mechanical properties of these crystals [36].

The higher valence band consists of several distinct peaks, in which the smallest peak at the left in M_2SnC excluding Lu_2SnC originates as a result of weak interaction of d-orbitals of M atoms and p-orbitals of C and Sn atoms. At the similar energy position, an extra-large peak (also shown in inset) is observed in the higher valence band of Lu_2SnC, which is responsible for a wide flat band in the band structure. The next peak in Ti, Nb, Hf and Zr based M_2SnC phases is their highest peak and arises due to the hybridization between M d and C p orbitals. This hybridization strengthens the covalent M-C bonding. In the last one, the main contribution comes from M d and Sn p states of all the studied phases. In Lu_2SnC phase, the C p states contribute equally. This interaction leads to weaker covalent M-Sn bonding owing to proximity of the peak to the Fermi level. Therefore, the overall bonding nature in the studied M_2SnC MAX phases should be a combination of metallic, covalent, and, due to the difference in electronegativity between the constituent atoms, ionic.

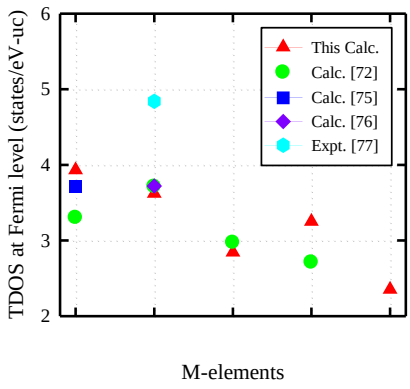

Fig. 8. Total density of states (TDOS) at Fermi level of M_2SnC MAX phases.

3.2 Mulliken atomic population analysis

Mulliken atomic population analysis is the most common and simplest method for analyzing the atomic population. This method assigns charges to wave functions represented in LCAO basis sets and gives an effective way to quantify the atomic charge, effective valence, charge transfer, etc. Mulliken atomic charge on the anion species facilitates the calculation of the effective valence from the formal ionic charge. The effective valence of an atomic species defined as the difference between formal ionic charge and Mulliken atomic charge can quantify the degree of covalency or ionicity of a chemical bond. Small values of effective valence correspond to an ionic bond, while a purely ionic bond assigns with a zero value. Actually, the increase of effective valence from zero value leads to decrease of ionicity and increase of covalency. The calculated effective valence for newly synthesized Lu_2SnC and its analogues M_2SnC (M = Ti, Nb, Hf, Zr) is presented in Table 1, indicating the dominant covalency in their chemical bonding.

Mulliken charge analysis also estimates the charge transfer from one atom to another. In the Ti_2SnC crystal, the amount of charge transferred to the C and Sn from Ti is 0.74 and 0.11e, respectively. Likewise, the charge transfer from Zr to C and Sn is 0.78 and 0.07e, respectively for Zr_2SnC. In the case of Lu_2SnC, the electron charge of 0.43 and 0.46 is transitioned to the C and Sn from Lu, respectively. In Nb_2SnC and Hf_2SnC, Sn takes part in charge transferring instead of charge receiving. Only C atoms receive 0.68 and 0.86e charges from M (Nb/Hf) and Sn atoms, respectively in these two ternary carbides. The charge transferring in M_2SnC phases is responsible for their ionic nature in chemical bonding.

Bond length is another measure of bond strength. The shorter the bond length, the stronger the chemical bond. The calculated bond length is shown in Table 2. Evidently, the strength of M–C bond is much stronger than that of M–Sn bond. M–C bond is more covalent than M–Sn bond. Considering both the covalent bonds, the covalency in M_2SnC crystals follows the order Ti_2SnC > Nb_2SnC > Hf_2SnC > Zr_2SnC > Lu_2SnC. This order is opposite to the order of crystal radius of M_2SnC solids. Therefore, it can be concluded that the bond length is proportional to the crystal radius (see Fig. 9), while bond covalency is inversely proportional to the crystal radius.

Table 1. Effective valence, Mulliken charge and atomic populations for M_2SnC MAX phases.

Phase	Species	No. of ions	s	p	d	f	Total	Charge (e)	Effective valence (e)
Ti_2SnC	Ti	4	2.19	6.68	2.71	0.00	11.58	0.42	3.58
	Sn	2	1.54	2.57	0.00	0.00	4.11	-0.11	3.89
	C	2	1.47	3.27	0.00	0.00	4.74	-0.74	3.22
Nb_2SnC	Nb	4	2.23	6.48	3.98	0.00	12.69	0.31	4.69
	Sn	2	1.49	2.44	0.00	0.00	3.93	0.07	3.93
	C	2	1.45	3.24	0.00	0.00	4.68	-0.68	3.32
Hf_2SnC	Hf	4	0.47	0.40	2.85	0.00	3.72	0.28	3.72
	Sn	2	1.05	2.64	0.00	0.00	3.69	0.31	3.69
	C	2	1.55	3.32	0.00	0.00	4.86	-0.86	3.14
Zr_2SnC	Zr	4	2.26	6.56	2.75	0.00	11.57	0.43	3.57
	Sn	2	1.52	2.56	0.00	0.00	4.07	-0.07	3.93
	C	2	1.49	3.29	0.00	0.00	4.78	-0.78	3.22
Lu_2SnC	Lu	4	0.38	6.01	1.91	14.25	22.55	0.45	2.55
	Sn	2	1.57	2.89	0.00	0.00	4.46	-0.46	3.54
	C	2	1.33	3.11	0.00	0.00	4.43	-0.43	3.57

Table 2. Calculated bond lengths for M_2SnC with (M = Ti, Nb, Hf, Zr, and Lu).

	M-C		Sn-C		M-Sn	
Compounds	This Calc.	Calc. [72]	This Calc.	Calc. [72]	This Calc.	Calc. [72]
Ti_2SnC	2.14139	2.126	3.90027	3.861	2.96600	2.923
Nb_2SnC	2.20031	2.193	3.95511	3.915	3.00095	2.963
Hf_2SnC	2.31581	2.270	4.12331	4.086	3.07137	3.055
Zr_2SnC	2.31179	2.302	4.16312	4.150	3.11272	3.100
Lu_2SnC	2.42779	-----	4.34473	-----	3.25484	-----

.

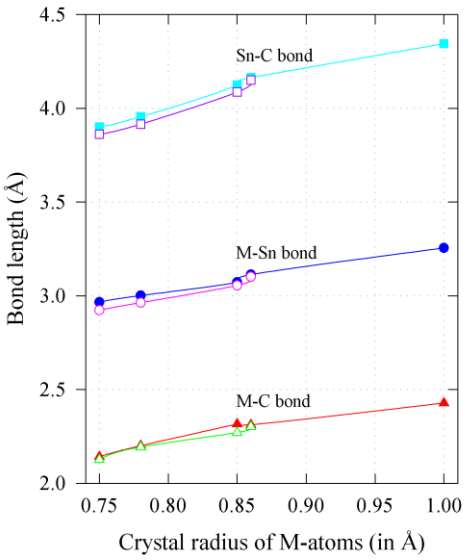

Fig. 9. Bond length in M_2SnC as a function of crystal radius of M-atoms. Filled and open symbols respectively represent the values obtained in present study and literature [72].

3.3 Electron charge density and Fermi surface

The contour maps of electron charge density for Sn-containing five 211 MAX phases are investigated to further understand their chemical bonding and presented in Fig. 10. The charge distributions around M atoms are almost spherical and their intensity indicates the amount of charge accumulation. Evidently, the lowest charge is accumulated around the Hf atom (0.28e), while the highest charge is deposited around the Lu atom (0.45e). The amount of Mulliken charge on M-atoms follow the order, Lu > Zr > Ti > Nb > Hf. This charge fairly overlaps with the C-charge and slightly edges with the Sn-charge, indicating stronger M–C and weaker M–Sn bonds, respectively. The spherical nature of charge distributions also indicates some ionic characters in chemical bonds in M_2SnC MAX phases, fairly Sn–C bond.

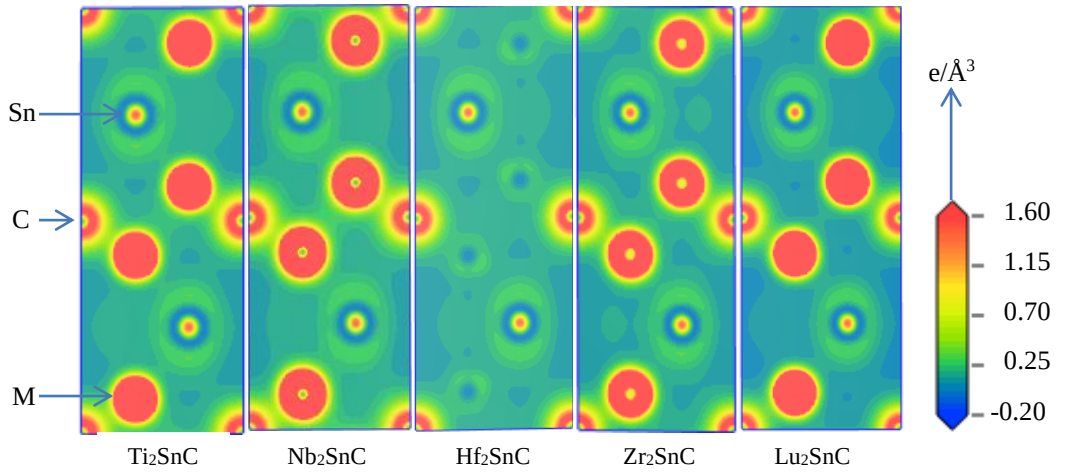

Fig. 10. Electron charge density map of M_2SnC MAX phases

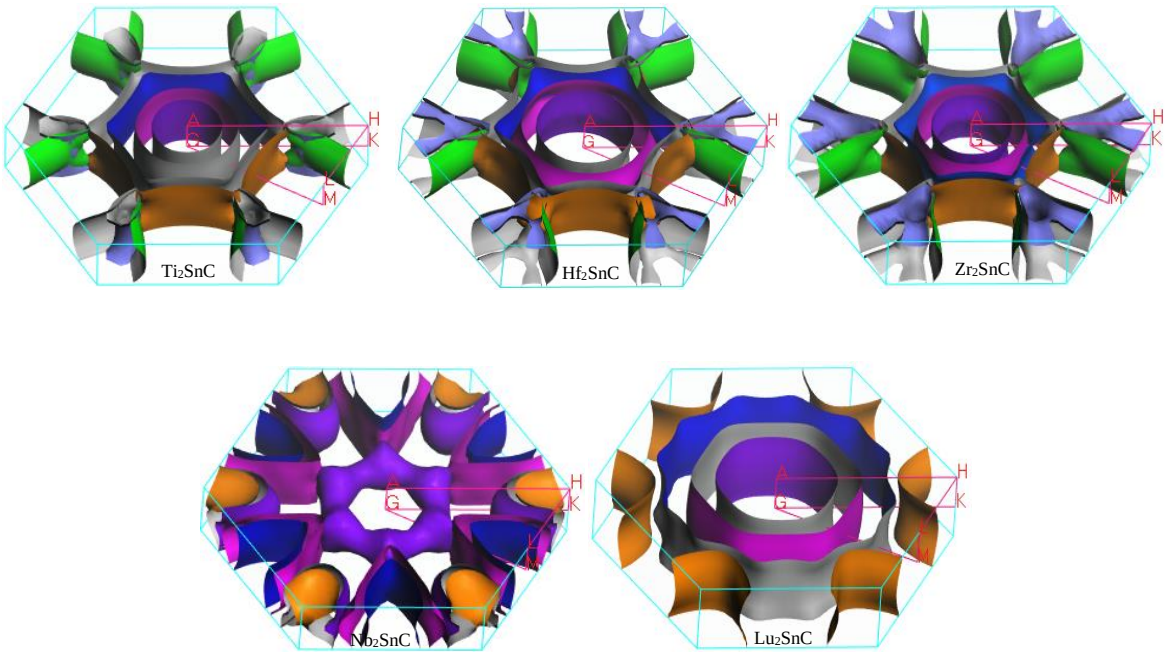

Fig. 11. Fermi surfaces of M_2SnC MAX phases

Fermi surface, a conceptual geometrical presentation of all the available electronic states, aids in characterizing a material and its thermal, electrical, and magnetic properties. To develop a material with desired functionality, the knowledge of Fermi surface can help the material scientists. The calculated Fermi surfaces of newly synthesized Lu_2SnC and its isostructural existing M_2SnC (M = Ti, Nb, Hf and Zr) 211 MAX phases are presented in Fig. 11.

The Fermi surface topologies of Ti_2SnC, Hf_2SnC and Zr_2SnC look like almost identical. They are also comparable with those of their 312 MAX phase counterparts [44]. These topologies contain different sheets. First four sheets are seen to be centered along the Γ-A direction and reveal the electron characteristics. The first sheet is cylindrical and the other three sheets are prismatic-like with hexagonal cross sections. There are two hole-like sheets with complex topology at the corners of the Brillouin zone around the H-K directions.

Among the five studied M_2SnC phases, Nb_2SnC and Lu_2SnC are superconducting compounds. So, we would expect that the features of the Fermi surfaces of these two MAX superconductors will be identical. It is surprising that there is no common feature in the Fermi surfaces of these compounds. It can be assumed that the different origin of superconductivity in Nb_2SnC and Lu_2SnC leads to form their dissimilar Fermi surfaces. The properties of superconducting state are strongly dependent on the synthesis method [76]. The Fermi surface topology of Lu_2SnC is quite different from those of the non-superconducting phases Ti_2SnC, Hf_2SnC and Zr_2SnC. There is no prismatic sheet in the Fermi surface of Lu_2SnC. The Fermi surface topology of Lu2SnC is most simple compared to those of other M_2SnC phases.

3.4. Defect processes

Table 3 reports the intrinsic defect processes (in Kröger–Vink notation [78], in this notation V_C and C_i represent a C vacancy and C interstitial atom respectively) and the relative energies for the M_2SnC phases considered. The first three reactions are the Frenkel defects and these can be deemed as important particularly for nuclear applications. This is because low Frenkel energies can be linked to higher concentrations of persistent defects. The lowest energy Frenkel process is the carbon Frenkel (reaction 3, Table 3). For these MAX phases the Schottky defect processes are significantly higher in energy as compared to the C-Frenkel process (refer to Table 3).

Table 3. The defect reaction energies as calculated for the various M_2SnC MAX phases (M = Lu, Ti, Zr, Hf, Nb)

	Reaction	Defect energy (eV)				
		Lu_2SnC	Ti_2SnC	Zr_2SnC	Hf_2SnC	Nb_2SnC
1.	$M_M \rightarrow V_M + M_i$	6.61	8.75	8.66	9.34	8.70
2.	$Sn_{Sn} \rightarrow V_{Sn} + Sn_i$	3.57	8.97	6.63	7.51	7.56
3.	$C_C \rightarrow V_C + C_i$	2.23	6.10	5.34	4.68	5.18
4.	$M_M + Sn_{Sn} \rightarrow M_{Sn} + Sn_M$	3.67	4.92	4.83	4.72	5.12
5.	$M_M + C_C \rightarrow M_C + C_M$	11.79	12.81	15.40	16.37	12.64
6.	$Sn_{Sn} + C_C \rightarrow Sn_C + C_{Sn}$	7.75	9.98	9.64	10.07	10.05
7.	$Sn_i + V_M \rightarrow Sn_M$	-3.61	-6.86	-4.71	-5.17	-4.34
8.	$C_i + V_M \rightarrow C_M$	-0.13	-1.07	0.12	1.47	-0.48
9.	$M_i + V_{Sn} \rightarrow M_{Sn}$	-2.90	-5.94	-5.75	-6.96	-6.79
10.	$C_i + V_{Sn} \rightarrow X_{Sn}$	1.56	-0.19	0.22	0.89	-0.10
11.	$M_i + V_C \rightarrow M_C$	3.08	-0.97	1.28	0.88	-0.76
12.	$Sn_i + V_C \rightarrow Sn_C$	0.39	-4.91	-2.55	-3.01	-2.58
13.	$M_i + Sn_{Sn} \rightarrow M_{Sn} + Sn_i$	0.67	3.03	0.88	0.55	0.76
14.	$M_i + C_C \rightarrow M_C + C_i$	5.31	5.13	6.62	5.56	4.42
15.	$Sn_i + M_M \rightarrow Sn_M + M_i$	3.01	1.89	3.95	4.17	4.36
16.	$Sn_i + C_C \rightarrow Sn_C + C_i$	2.62	1.19	2.79	1.67	2.60
17.	$C_i + M_M \rightarrow C_M + C_i$	6.49	7.69	8.78	10.81	8.22
18.	$C_i + Sn_{Sn} \rightarrow X_{Sn} + Sn_i$	5.13	8.79	6.85	8.40	7.46
	Schottky reaction	9.99	7.97	9.69	8.57	6.70

Antisite defects are common defects in these materials and can have non-negligible concentrations particularly in a radiation environment. Typically, in a radiation environment the non-equilibrium point defects can either recombine or occupy alternative lattice site to form antisites [79,80]. Low antisite formation energies are indicative that an important proportion of antisites will remain in the host lattice [79,80]. The common antisite formation mechanisms are relations 4-6 in Table 3. The antisite defect formation reactions 5 and 6 have very high energies and are not relevant. Reaction 4 with energies ranging from 3.67 eV (Lu_2SnC) to 5.12 (Nb_2SnC) may become significant particularly for Ti_2SnC, Zr_2SnC and Nb_2SnC for which it is lower in energy than the Frenkel processes. Interestingly, for Hf_2SnC and Nb_2SnC the antisite and C-Frenkel reactions have very similar energies and these processes will both play a role simultaneously.

Reactions 7-12 (Table 3) reveal whether interstitial defects will associate with vacant sites to form antisite defects or remain as isolated defects. For all the MAX phases considered here Sn_i will associate with V_M to form Sn_M (reaction 7) and M_i will interact with V_{Sn} to form M_{Sn} (reaction 9). For the other reactions there is no clear trend but Table 3 can serve as a guide of the possible defects that can form.

Finally, we considered the displacement of lattice atoms by interstitials to form antisite defects (reactions 13-18). This is particularly relevant under irradiation, where a non-equilibrium concentration of interstitials can exist. This route for the formation of antisite defects in the M_2SnC MAX phases is deemed to be energetically unfavourable (refer to Table 3). Nb_2SnC has a higher energy for its lowest energy defect process (i.e. Schottky or Frenkel) as compared to the other MAX phases considered here. Therefore, Nb_2SnC should have better radiation tolerance among studied M_2SnC phases.

4. Conclusions

DFT calculations were performed in order to calculate the electronic structure, bonding natures and energetics of the intrinsic defect processes of M_2SnC (M = Lu, Ti, Zr, Hf, Nb) MAX phases. The calculated formation energies of M_2SnC are negative, signifying that these compounds are intrinsically stable in accordance with the experiment. The band profiles of M_2SnC are distinctive in shape though all they indicate the metallic conductivity. The covalency in M_2SnC decreases as the M-atom moves from Ti to Lu following the order Ti $\rightarrow$ Nb $\rightarrow$ Hf $\rightarrow$ Zr $\rightarrow$ Lu. Lu_2SnC is predicted to be softer than other studied M_2SnC phases. The charge transfer in M_2SnC as well as the spherical nature of charge distributions in contour maps of electronic charge indicates the ionic character of chemical bonds. Basically, the chemical bonds in studied M_2SnC phases are a combination of ionic, metallic and covalent in nature. The bond length and bond covalency are directly and inversely proportional to the crystal radius, respectively. The dissimilar Fermi surfaces of Nb_2SnC and Lu_2SnC indicate the different origin of superconductivity in these two MAX phases. For Ti_2SnC, Zr_2SnC and Nb_2SnC the dominant intrinsic disorder mechanism was calculated to be the antisite mechanism (reaction 4, Table 3), whereas for Lu_2SnC and Hf_2SnC the C Frenkel (reaction 4, Table 3). Other intrinsic defect processes are less significant. Based only on the intrinsic defect processes Nb_2SnC is the material that should have the better radiation tolerance of the M_2SnC MAX phases (M = Lu, Ti, Zr, Hf, Nb) considered here.

Data Availability: Supplementary data will be made available on request.

Author Contributions:

M.A.H. and N.K. performed the first-principles calculations. M.A.H. and A.C. wrote the manuscript and discussed the results. S.H.N. designed the project and supervised along with A.C. and A.K.M.A.I. All authors revised the manuscript.

Reference

[1] M. W. Barsoum, Prog. Solid. State Chem. **28** (2000) 201–281.

[2] W. Jeitschko, H. Nowotny, and F. Benesovsky, Monatsch. Chem. **94** (1963) 672.

[3] M. W. Barsoum and T. El-Raghy, J. Am. Ceram. Soc. **79** (1996) 1953–1956.

[4] M. W. Barsoum, L. Farber, I. Levin, A. Procopio, T. El-Raghy, and A. Berner, J. Am. Ceram. Soc. **82** (1999) 2545–2547.
[5] A.T. Procopio, T. El-Raghy, and M.W. Barsoum, Metall. Mater. Trans A 31A (2000) 373–378.
[6] A.T. Procopio, M.W. Barsoum, and T. El-Raghy, Metall. Mater. Trans A 31A (2000) 333–337.
[7] M. W. Barsoum and T. El-Raghy, American Scientist, 89 (2001) 334–343.
[8] M. F. Cover, O. Warscgkov, M. M. M. Bilek, and D. R. Mckenzie, J. Phys.: Condens. Mater 21 (2009) 305403.
[9] O. Eklund, M. Beckers, U. Jansson, H. Hogberg, and L. Hultman, Thin Solid Films 518 (2010) 1851–1878.
[10] M. W. Barsoum and M. Radovic, Annu. Rev. Mater. Res. 41 (2011) 195–227.
[11] Z. M. Sun, International Materials Research 56 (2011) 143–166.
[12] S. Aryal, R. Sakidja, M. W. Barsoum, and W.-Y. Ching, Phys. Stat. Solidi B 251 (2014) 1480–1497.
[13] C. Dhakal, S. Aryal, R. Sakidja, and W.-Y. Ching, J. Eur. Ceram. Soc 35 (2015) 3203–3212.
[14] H. Yoo, M.W. Barsoum, T. El-Raghy, Nat. Lond. 407 (2000) 581.
[15] T. El-Raghy, et al., J. Am. Ceram. Soc. 82 (1999) 2855.
[16] M.W. Barsoum, L. Farber, T. El-Raghy, Metall. Mater. Trans. A 30 (1999) 1727.
[17] Z.M. Sun, et al., Mater. Trans. 47 (2006) 170.
[18] P. Finkel, M.W. Barsoum, T. El-Raghy, J. Appl. Phys. 87 (2000) 1701.
[19] M.W. Barsoum, Physical Properties of the MAX Phases, Encyclopedia of Materials: Science and Technology, Elsevier, Amsterdam, 2009.
[20] M. Radovic, et al., J. Alloys Compd. 361 (2003) 299.
[21] C.J. Gilbert, et al., Scr. Mater. 238 (2000) 761.
[22] M. Sundberg, et al., Ceram. Int. 30 (2004) 1899.
[23] D. Horlait, S. Grasso, A. Chroneos, W.E. Lee, Mater. Res. Lett. 4 (2016) 317
[24] D.J. Tallman, Mater. Res. Lett. **1** (2013) 115.
[25] A. Farle, Smart Materials and Structures **25** (2016) 1.
[26] E. Hoffman, Nuclear Engineering and Design. **244** (2012) 17.
[27] E. Hoffman, Microporous and Mesoporous Materials. **112** (2008) 526–532.
[28] M. Naguib, Advanced Materials. **23** (2011) 4248–4253.
[29] Z.M. Sun, Int. Mater. Reviews 56 (2011) 143–166.
[30] M.A. Hadi, Comp. Mater. Sci. 117 (2016) 422–427.
[31] T. Lapauw, K. Lambrinou, T. Cabioc'h, J. Halim, J. Lu, A. Pesach, O. Rivin, O. Ozeri, E.N. Caspi, L. Hultman, P. Eklund, J. Rosen, M.W. Barsoum, J. Vleugels, J. Eur. Ceram. Soc. 36 (2016) 1847–1853.
[32] T. Lapauw, B. Tunca, T. Cabioc'h, J. Lu, P.O.Å. Persson, K. Lambrinou, J. Vleugels, Inorg. Chem. 55 (2016) 10922–10927.

[33] T. Lapauw, J. Halim, J. Lu, T. Cabioc'h, L. Hultman, M.W. Barsoum, K. Lambrinou, J. Vleugels, J. Eur. Ceram. Soc. 36 (2016) 943–947.

[34] T. Lapauw, B. Tunca, T. Cabioc'h, J. Vleugels, K. Lambrinou, J. Eur. Ceram. Soc. 37 (2017) 4539–4545.

[35] S. Kuchida, T. Muranaka, K. Kawashima, K. Inoue, M. Yoshikawa and J. Akimitsu, Physica C 494 (2013) 77–79.

[36] M.A. Hadi, N. Kelaidis, S.H. Naqib, A. Chroneos, A.K.M.A. Islam, J. Phys. Chem. Solids. 129 (2019) 162–171.

[37] S. J. Clark, M. D. Segall, C. J. Pickard, P. J. Hasnip, M. I. J. Probert, K. Refson, and M. C. Payne, Z. Kristallogr. 220 (2005) 567.

[38] P. Hohenberg and W. Kohn, Phys. Rev. 136 (1964) B864.

[39] W. Kohn and L.J. Sham, Phys. Rev. 140 (1965) A1133.

[40] J.P. Perdew, K. Burke, and M. Ernzerhof, Phys. Rev. Lett. 77 (1996) 3865.

[41] D. Vanderbilt, Phys. Rev. B 41 (1990) 7892.

[42] H. J. Monkhorst and J. D. Pack, Phys. Rev. B 13 (1976) 5188.

[43] T.H. Fischer and J. Almlof, J. Phys. Chem. 96 (1992) 9768.

[44] M.A. Hadi, S.-R.G. Christopoulos, S.H. Naqib, A. Chroneos, M.E. Fitzpatrick, A.K.M.A. Islam, J. Alloys Comp. 748 (2018) 804-813.

[45] A.M.M. Tanveer Karim, M.A. Hadi, M.A. Alam, F. Parvin, S.H. Naqib, A.K.M.A. Islam, J. Phys. Chem. Solids 117 (2018) 139–147.

[46] S.-R. G. Christopoulos, P. P. Filippatos, M. A. Hadi, N. Kelaidis, M. E. Fitzpatrick, A. Chroneos, J. Appl. Phys. 123 (2018) 025103.

[47] M.T. Nasir, M.A. Hadi, ..., S.H. Naqib, A.K.M.A. Islam, M. M. Uddin, K. Ostrikov, Phys. Status Solidi B 254 (2017) 1700336.

[48] M. Roknuzzaman, M.A. Hadi, M.A. Ali, M.M. Hossain, ..., J.A. Alarco, K. Ostrikov, J. Alloys Comp. 727 (2017) 616-626.

[49] M.A. Hadi, S.H. Naqib, S.-R.G. Christopoulos, A. Chroneos, A.K.M.A. Islam, J. Alloys Comp. 724 (2017) 1167-1175.

[50] Mirza H.K. Rubel, M.A. Hadi, M.M. Rahaman, ..., A.K.M.A. Islam, N. Kumada, Comp. Mater. Sci. 138 (2017) 160–165.

[51] M.A. Hadi, M. Roknuzzaman, A. Chroneos, S.H. Naqib, A.K.M.A. Islam, R.V. Vovk, K. Ostrikov, Comp. Mater. Sci. 137 (2017) 318–326.

[52] E. Zapata-Solvas, M.A. Hadi,....., A. Chroneos, W.E. Lee, J. Am. Ceram. Soc. 100 (2017) 3393–3401.

[53] M.A. Ali, M.A. Hadi, M. M. Hossain, S.H. Naqib, A.K.M.A. Islam, Phys. Stat. Solidi B 254 (2017) 1700010.

[54] M.A. Hadi, M.S. Ali, S.H. Naqib, A.K.M.A. Islam, Chin. Phys. B 26 (2017) 037103.

[55] M.A. Hadi, Y. Panayiotatos, A. Chroneos, J. Mater. Sci.: Mater. Electronics 28 (2017) 3386–3393.

[56] M.A. Hadi, R. V. Vovk, A. Chroneos, J. Mater. Sci.: Mater. Electronics 27 (2017) 11925-11933.

[57] M.A. Hadi and M S Ali, Chin. Phys. B 25 (2016) 107103.

[58] M.A. Hadi, M.T. Nasir, M. Roknuzzaman, M.A. Rayhan, S.H. Naqib, A.K.M.A. Islam, Phys. Stat. Solidi B 253 (2016) 2020–2026.

[59] M.A. Alam, M.A. Hadi, M.T. Nasir, M. Roknuzzaman, F. Parvin, M. A. K. Zilani, A.K.M.A. Islam, S.H. Naqib, J. Supercon. Novel Magn. 29 (2016) 2503–2508.

[60] M. Roknuzzaman, M.A. Hadi, M. J. Abden, M. T. Nasir, A.K.M.A. Islam, M.S. Ali, K. Ostrikov, S.H. Naqib, Comp. Mater. Sci. 113 (2016) 148–153.

[61] M.A. Hadi, M.A. Alam, M. Roknuzzaman, M.T. Nasir, A.K.M.A. Islam, S. H. Naqib, Chin. Phys. B 24 (2015) 117401.

[62] M.T. Nasir, M.A. Hadi, S.H. Naqib, F. Parvin, A.K.M.A. Islam, M. Roknuzzaman, M.S. Ali, Int. J. Mod. Phys. B 28 (2014) 1550022.

[63] M. A. Hadi, M. S. Ali, S. H. Naqib, A. K. M. A. Islam, Int. J. Comp. Mater. Sci. Eng. 2 (2013) 1350007.

[64] M. A. Hadi, U. Monira, A. Chroneos, S. H. Naqib, A. K. M. A. Islam, N. Kelaidis, R. V. Vovk, J. Phys. Chem. Solids 132 (2019) 38-47.

[65] M.A. Hadi, M. N. Islam, M. H. Babu, Z. Naturforsch. A 74 (2019) 71.

[66] D. Sanchez-Portal, E. Artacho, and J. M. Soler, Soid State Commun. 95 (1995) 685.

[67] R.S. Mulliken, J. Chem. Phys. 23 (1955) 1833.

[68] D. Horlait, S. Middleburgh, A. Chroneos, W.E. Lee, Sci. Rep. 6 (2016) 18829.

[69] W. Jeitschko, H. Nowotny and F. Benesovsky, Monatsh. für Chem. 94 (1963) 672–676; Monatsh. für Chem. 95 (1964) 431–435

[70] M.W. Barsoum, G. Yaroschuck, and S. Tyagi, Scrip. Mater. **37** (1997) 1583–1591.

[71] S. Aryal, R. Sakidja, M. W. Barsoum, and W.-Y. Ching, Phys. Stat. Solidi B 251 (2014) 1480-1497.

[72] M.B. Kanoun, S. Goumri-Said, A.H. Reshak, Comp. Mater. Sci. 47 (2009) 491–500.

[73] A. Bouhemadou, Physica B 403 (2008) 2707.

[74] F. Birch, Phys. Rev. **71** (1947) 809–824.

[75] G. Hug, Phys. Rev. B 74 (2006) 184113.

[76] A.D. Bortolozo, O.H. Sant'Anna, M.S. da Luz, C.A.M. dos Santos, A.S. Pereira, K.S. Trentin, A.J.S. Machado, Solid State Commu. 139 (2006) 57–59.

[77] S.E. Loftand, J.D. Hettinger, K. harrell, P. Finkel, S. Gupta, M.W. Barsoum, and G. Hug, Appl. Phys. Lett. 84 (2004) 508.

[78] F. A. Kröger, and H. J. Vink, Relations between the concentrations of imperfections in crystalline solids. Solid State Phys. 3 (1956) 307-435.

[79] Sickafus, K. E., *et al.* Radiation tolerance of complex oxides. Science 289 (2000) 748-751.

[80] Middleburgh, S. C., Lumpkin, G. R. & Riley, D. Accommodation, accumulation, and migration of defects in Ti_3SiC_2 and Ti_3AlC_2 MAX phases. J. Am. Ceram. Soc. 96 (2013) 3196-3201.